

## **NUMERICAL INVESTIGATION FOR EVALUATION OF SEISMIC PERFORMANCE OF SMA-CONFINED STRUCTURAL ELEMENTS**

Arpita Ghosh

Postgraduate Student, Indian Institute of Technology Guwahati  
Guwahati-781039, India, Email: [arpit174104083@iitg.ac.in](mailto:arpit174104083@iitg.ac.in)

Anjan Dutta (Corresponding Author)

Professor, Indian Institute of Technology Guwahati  
Guwahati-781039, India, Email: [adutta@iitg.ac.in](mailto:adutta@iitg.ac.in)

### **ABSTRACT**

With the increased accentuation on both reliability and automation in the civil engineering field, the smart materials are quickly turning into an empowering innovation. One of these kinds is the shape memory alloy (SMA) with superior mechanical properties known as superelasticity (SE) and shape memory effect (SME), which enables them to recover permanent deformations when thermally activated. The SMAs can induce high recovery stresses owing to their SME property, which can be utilized to apply high and permanent confining pressures on concrete. Hence a numerical study was conducted to comprehend the performance of Fe-SMA-confined concrete cylinder and bridge pier specimens. Cylinder specimens for different design parameters were analyzed. Further bridge pier specimens were analyzed with the following layouts for retrofitting: externally bonded (EB), near-surface mounted (NSM), and hoop confinement. The particular focus of this study is on the aspects of finite element modeling and simulation of the behavior of SMA-confined concrete and show the feasibility of this technique in strengthening RC bridge columns. 3D non-linear finite element analysis were carried out in ABAQUS with concrete damaged plasticity model to predict and study the behavior of SMA-confined concrete cylinder under uniaxial compression and bridge piers under cyclic loading. This result presents the parametrical analyses on the effects of an increase in active confinement level and geometric parameters of cylinders and bridge pier. The results show that RC structures confined with Fe-SMA strips have significantly improved capacity when compared with those of the as-built structures.

**KEYWORDS:** Fe-SMA Confinement, Numerical Investigation, RC Structure, Seismic Performance

### **INTRODUCTION**

Damages from past earthquakes boost the demand for growing new methodologies and advances to improve the existing infrastructure performance in the event of earthquakes. Bridges being an integral component of the transportation infrastructure needs quick restoration to their full functioning after an earthquake hit to nullify interference with disaster recovery operations. The seismic design approach for bridges in this modern era involve the use of capacity design principles that locate plastic hinges in columns while protecting against other locations of damages [1]. Therefore, bridge columns should remain functional with minimal damage in order to avoid hindrance with recovery work. Owing to their strategic importance, quick restoration after an earthquake hit is the need of the hour. Several techniques for the repair and strengthening of bridge columns have been developed in the past four decades. Numerous experimental and analytical studies advocate the role of lateral confinement in increasing the strength as well as deformability of concrete structures, especially compression members [2-5]. Lateral confinement can be broadly divided into passive confinement [6-8], such as concrete jackets, FRP jackets, and active confinement [9-11], such as prestressed steel bands or FRP wraps. A particularly innovative avenue of research is that of confinement methods which engage the use of active confining forces. It fosters on the fact that where passive confinement methods rely on dilating concrete due to load application to initiate the generation of confining pressures, active confinement methods apply an initial confining pressure through prestressing, resulting in confinement being effective before actually, the loading begins.

Many attempts of active confinement with the regular materials which are used in passive confinement had been investigated in literature. Saatcioglu et al. [12] observed through experimental investigations on large column specimens that the use of prestressing wire strands as hoops could be an effective strategy to

improve shear capacity and ductility. Nasrollahzadeh et al. [13] worked on damaged concrete columns and retrofitted them using pre-tensioned FRP belts. Improved flexural, as well as the shear capacity of those considered damaged column specimens, were observed. Although these active confining methods proved to be quite efficient, the limitation lies in the application of mechanical prestress in terms of required labour, time, and cost. Therefore, a substitute to overpower these difficulties known as shape memory alloy was investigated in this study for active confinement of RC structures. The Shape Memory Alloys (SMA) are superelastic (SE) alloys having a unique trait of remembering their original shape, which they can recover if subjected to determinate characteristic temperatures, the property which is well known as shape memory effect (SME). With these interesting properties (SE and SME), a temporary deformed shape can be virtually held always until the right stimulus (primarily temperature) is applied to activate a shape recovery and return the alloy back to the original undeformed shape. Because of this reversible process, SMAs have an endless measure of conceivable applications and have all the earmarks of being one of the fundamental smart materials of things to come. The SME these alloys exhibit is due to the thermomechanical phase transformation from austenite to martensite. Starting from the discovery in 1932 by Chang and Read, this alloy has developed significantly and had been in practical use in many science and engineering fields. Currently, three major variants of SMA alloys exist: nickel titanium based (NiTi), copper-based (Cu-Al-Ni and Cu-Zn-Al), and iron-based (Fe-Mn-Si, Fe-Ni-C and Fe-Ni-Co-Ti) of which the NiTi based alloys having a third component are the most dominant in use [14]. Literature proves the advent of SMAs to be very beneficial in the civil engineering field. By far, many researchers have studied NiTiNb-SMAs for active control, damping, and pre-stressing strengthening material, and many more. But since the cost is a major concern, a cheaper substitute is needed. From the recent findings, it has been evident that iron-based SMAs (Fe-SMA) such as Fe-Mn-Si based alloys seem to be more feasible for structural applications due to their low cost. Dong et al. [15] reported a novel Fe-Mn-Si based alloy with VC precipitates as a low-cost alternative to NiTi. The composition of this novel alloy is Fe-17Mn-5Si-10Cr-4Ni-1 (VC), with a transformation temperature of 162°C and a stress recovery of about 330 MPa [15].

Andrawes et al. [16] were the first to present the idea of seismic retrofit of bridge columns using this pioneering technique of wrapping wires around the specimens. Later Andrawes et al. [17] carried out experimental and analytical work to showcase the feasibility of using spirals made of NiTiNb-SMAs for seismic retrofitting of RC bridge columns. They also performed tests of uniaxial compression on concrete cylinders confined with SMA wires. The performance of the SMA retrofitted column was compared with that of carbon fiber-reinforced polymer (CFRP) retrofitted column. The analytical results shows that the performance of RC columns retrofitted with SMA spirals was substantially improved compared to the CFRP retrofitted column in increasing the strength and effective stiffness and reducing the plastic deformations. The practical application of SMAs in enhancing the ductility performance of reinforced concrete bridge columns during earthquakes was also analyzed by Shin et al. [18]. Their compression test results indicated the effectiveness of SMAs in applying active confining pressure on the tested concrete specimens. Shin et al. [19] also performed experiments to investigate the seismic performance of reinforced concrete (RC) columns by SMAs, passively confined with GFRP sheets and combining both under quasi-static cyclic loading. The results dictated a significant increase in the energy dissipation and ductility of the column wrapped with SMA spirals compared to that with GFRP sheets. Chen et al. [20] developed a finite element model to analyze the behavior of SMA and GFRP-SMA-confined concrete under uniaxial compression load. They used NiTiNb, SMAs as transverse reinforcement to confine concrete for enhancing strength and ductility. The parametric study revealed reduced spacing of SMA and increased thickness of GFRP and their combination used as confinement to concrete specimens can provide higher active confining pressure, higher concrete peak stress and higher residual stress. Note that for real engineering projects lower cost SMAs like iron-based shape memory alloys as compared to NiTi based alloys can be good candidate for commercialisation. The groundwork by Shahverdi et al. [21] concentrates on the application Fe-SMAs in the field of civil engineering. They conducted sizeable experimental studies to examine Fe-SMA's physical behavior and characterized its mechanical properties for shape memory effect at ambient temperature. Their study states a prestraining level of 2% to be the optimal choice to induce recovery behavior of Fe-SMAs. Lee et al. [22] investigated thermo-mechanical behaviour of Fe-17Mn-5Si-10Cr-4Ni-1(V, C) (ma.-%) shape memory alloy and illustrated the different phase transformation and encompassing temperatures to trigger their SME effect. Shahverdi et al. [23] experimentally studied the flexural behavior of reinforced concrete (RC) beams strengthened and prestressed with iron based SMA strips. Their results depicts higher cracking loads and lower mid-span deflection. Abouali et al. [24] carried

out finite element analysis in ABAQUS to examine the outcome of retrofitting of RC beams with Fe-SMA fixed as near-surface mounted (NSM) under bending.

Some of the recent works carried out under the theme of Fe-SMAs are listed further. Fritsch et al. [25] presented a detailed development process of the fastening technique for strengthening of steel members using Fe-SMA strips. Ghafoori et al. [26] carried out a systematic study for the evaluation of the behaviour of Fe-SMA strengthened structural members under the action of fire load in addition to the imposed service load. Li et al. [27] used NiTi shape memory alloy wires and CFRP sheets to produce a heat-activated pre-stressed SMA-CFRP composite patch for strengthening of cracked steel plates. Radd and Parvin [28] carried out finite element analysis for strengthening of reinforced concrete (RC) beams by pre-stressed fibre reinforced polymers and Fe-SMAs using the near-surface mounted technique. Cladera et al. [29] carried out external shear strengthening of large span RC beams using Fe-SMA strips with a U-configuration.

By far, limited research in numerical modelling of RC structures with Fe-SMA has been done. Therefore, this area needs to be evolved more so as to diversify the modelling method. In this study, a 3D FE model was selected in ABAQUS and used to study the behaviour of SMA-confined RC structures with concrete damaged plasticity model, which considers the concrete non-linear behavior. A modified constitutive model for confined concrete on account of confinement effect was selected. An initial stress was applied to prestress the Fe-SMA strips to define the recovery stress effect via a predefined field in ABAQUS. The Fe-SMA stress-strain curve applied to the FE model was simplified by including prestraining and recovery stress effect by implementing only the loading to failure part of the curve. The FE model shows the behaviour of RC structures under monotonic and cyclic loading when strengthened with Fe-SMA strips. Initially, the model was validated with experimental results of retrofitted RC beam prestressed with Fe-SMA strips as NSM reinforcement from Shahverdi et al. [23]. Then different design parameters such as active confinement levels, h/d ratio, and diameter of specimens were used to study the effectiveness of confining concrete cylinder specimens with Fe-SMA strips. Further, the study was evolved to analyse the effect of Fe-SMA retrofitted bridge piers with different strengthening layouts of Fe-SMA strips.

## RESEARCH SIGNIFICANCE

The use of Fe-SMAs for retrofitting of RC specimens is likely to enhance the performances in terms of load carrying capacity, ductility, energy dissipation, rate of degradation etc. However, different configurations related to the application of SMAs and other associated parameters are also likely to influence the effectiveness of its application. Thus, finite element based simulation studies are proposed to be used for the evaluation of the best possible combination of geometrical configuration, spacing and dimensional parameters of SMAs, while ensuring the improvement of the above-mentioned parameters.

## WORKING PRINCIPLE OF Fe-SMA

The prestressing principle of concrete structures with Fe-SMA strips comprises of three fundamental steps: Pre-straining, Activation via ambient temperature, and Service loading. A schematic portrayal of prestressing principle has been reported in the work of Shahverdi et al. [21]. The recovery stress is produced by increment and then decrement in temperature values while the Fe-SMA strip is restrained from any movement. The SME effect (i.e., the recovery stress generation) witnessed by Fe-SMAs is because of the stress-induced martensite transformation at room temperature. The reverse transformation is exhibited when heated beyond the transformation temperature. When temperature increment is started, thermal expansion occurs in SMA. The phase transformation starts at austenite start temperature. The tensile stresses generated in the SMA strips induce compressive stresses in the concrete element. When the temperature is decreased, further compressive stresses develop in the concrete element because of SMA thermal contraction. The mechanical phase change temperatures for Fe-SMA, reported by Lee et al. [22], are as follows: martensite finish ( $M_f$ )= 64°C, martensite start ( $M_s$ )= 60°C, austenite start ( $A_s$ )= 103°C, and austenite finish ( $A_f$ )= 163°C.

In this study for external Fe-SMA hoops, the effective active lateral confinement pressure was determined utilizing a modified version of the analytical stress-strain model by Mander et al. [4]. Effective active confinement depends on the recovery stress and the spacing of the SMA hoop confinement. The analytical stress-strain model by Mander et al. [4] for concrete confined with transverse steel reinforcement was extended to calculate confining pressure applied by SMA on concrete. This model assumes a uniform

distribution of lateral pressure from the transverse reinforcement into the concrete's surface. Therefore, it well justifies the externally confined concrete scenario with SMA reinforcement due to the recovery force generated.

$$\text{Lateral confining pressure, } f_l = \frac{2f_h A_{sp}}{s d_s} \quad (1)$$

where,  $f_h$  is recovery stress by SMA;  $A_{sp}$  is SMA strip cross-section area;  $d_s$  is section diameter;  $s$  is the pitch of spiral.

## FINITE ELEMENT MODELLING AND ANALYSIS

The FE model was developed herein by utilizing the method proposed by Abouali et al. [24] with few modifications.

**Elements Used:** The linear brick element (C3D8R) with reduced integration and hourglass control is used to model grout and concrete since they provide good results with the least computational effort [30]. For reinforcement, a 2-noded linear displacement truss element (T3D2) was used that can transmit only axial force. For the role of Fe-SMA strips, a 2-noded linear beam element (B31) with linear interpolation was selected, which is a Timoshenko beam element that accounts for transverse shear deformation [31]. A mesh size of 80 mm for the concrete, the reinforcements of the bridge pier, loading block, and foundation block was used. For the cylinder, 20 mm mesh size was used.

**Concrete Material Model:** For concrete material modeling in ABAQUS, the ‘‘Smearred crack concrete model’’ and the ‘‘Concrete Damaged Plasticity Model (CDPM)’’ can be used. For monotonic loading conditions smearred crack concrete model can be used. Whereas CDPM is used for monotonic, cyclic as well as dynamic loading conditions [31]. Besides, convergence problems are better-taken care of by CDPM when contrasted with the smearred crack model, which generally faces stress locking or other numerical problems causing convergence troubles [32]. In CDPM inelastic behavior of concrete is represented by isotropic damaged elasticity along with isotropic tensile and compressive plasticity [31]. The parameters required in CDPM are dilation angle, eccentricity, biaxial loading ratio, the coefficient  $K$  and viscosity parameter, concrete compressive and tensile constitutive relationship, and cracking and crushing damage parameters. A non-associated potential plastic flow rule is assumed. The flow potential used for CDPM is the Drucker-Prager hyperbolic function, the yield function of Lubliner et al. [33] with the modifications proposed by Lee et al. [34], which provides the evolution of strength under tension and compression [31]. The default plasticity parameter recommended by ABAQUS for CDPM was first used in the analysis. It was observed that the sensitivity of simulation was primarily regulated by two parameters of CDPM, namely, dilation angle and viscosity parameter. Hence, a sensitivity analysis was carried out for a viable range of dilation angle and viscosity parameter in ABAQUS, and accordingly, these values were adjusted to match the experimental results. The final values of CDPM parameters as adopted are shown in Table 1.

**Table 1: Concrete material model parameters**

Dilation angle	Eccentricity	$f_{bo} / f_{co}$	$K$	Viscosity parameter
31	1	1.16	0.667	0.0001
Concrete density (kg/m <sup>3</sup> )			Poisson's ratio	
2400			0.2	

The concrete compressive (cylinder) strength and direct tensile strength used from the CEB-FIP model code [35] are respectively:

$$f'_c = 0.85 f_{cu} \quad (2)$$

$$f_t = 0.33 \sqrt{f'_c} \quad (3)$$

where,  $f'_c$ ,  $f_{cu}$  and  $f_t$  are concrete compressive (cylinder), compressive (cube), and direct tensile strength, respectively. A modified concrete constitutive model for uniaxial compression using Hognestad parabola [36] with modification for effects of confinement [37] was used as described in the following equations. The equations for the concrete model in compression are given below:

$$\sigma_c^{(1)} = E_{c0} \varepsilon_c \quad \text{for } \sigma_c < 0.4 f'_c \quad (4)$$

$$\sigma_c^{(2)} = f_c' \left[ 2 \left( \frac{\varepsilon_c}{\varepsilon_c'} \right) - \left( \frac{\varepsilon_c}{\varepsilon_c'} \right)^2 \right] \quad \text{for} \left( \frac{\varepsilon_c}{\varepsilon_c'} \right) \leq 1 \quad (5)$$

$$\sigma_c^{(3)} = f_c' - \frac{f_c' (\varepsilon_c - \varepsilon_c')^2}{(\varepsilon_{c,max} - \varepsilon_c')^2} \quad \text{for} \left( \frac{\varepsilon_c}{\varepsilon_c'} \right) > 1 \quad (6)$$

where  $E_{c0}$  is elastic modulus,  $\varepsilon_c$  is the compressive strain,  $\varepsilon_{c,max}$  is the maximum strain of concrete and  $\varepsilon_c'$  is given as below:

$$\varepsilon_c' = \left( \frac{2f_c'}{E_{c0}} \right) \quad (7)$$

Since concrete in tension behaves almost linearly up to its tensile capacity with a slope of  $E_c$ , a linear ascending branch was considered for un-cracked concrete, after which stress decreased gradually to zero. The softening behavior for this descending branch was defined by the stress-crack opening displacement approach of ABAQUS CDPM using the exponential function derived by Cornelissen et al. [38] as given below:

$$\frac{\sigma}{f_t} = f(\omega) - \frac{\omega}{\omega_c} f(\omega_c) \quad (8)$$

$$f(\omega) = \left[ 1 + \left( \frac{c_1 \omega}{\omega_c} \right)^3 \right] \exp \left( - \frac{c_2 \omega}{\omega_c} \right) \quad (9)$$

$$\omega_c = 5.14 \frac{G_f}{f_t} \quad (10)$$

where  $\omega$  is the crack opening displacement,  $f(\omega)$  is a displacement function,  $\omega_c$  is the crack opening after which stress transfer can no longer take place,  $G_f$  is the concrete fracture energy. The values of material constants  $c_1$  and  $c_2$  for normal weight concrete, as suggested by Cornelissen et al. [38] were taken 3 and 6.93 respectively. The following concrete fracture energy equation as given in CEB-FIP model code [35] was used.

$$G_f = (0.0469d_a^2 - 0.5d_a + 26) \left( \frac{f_c'}{10} \right)^{0.7} \quad (11)$$

where  $d_a$  is the maximum size of aggregate, and  $f_c'$  is the compressive strength of concrete. The CDPM takes account of stiffness degradation due to compression damage and the post cracking damage with the help of damage parameters ( $d_c$  and  $d_t$ ). The evolution of compression degradation of concrete should be linked to plastic strain; hence equations proposed by Birtel and Mark [39] was used to define  $d_c$ .

$$d_c = 1 - \frac{\sigma_c E_c^{-1}}{\varepsilon_c^{pl} (1/b_c - 1) + \sigma_c E_c^{-1}} \quad (12)$$

where  $E_c$  is the modulus of elasticity,  $\sigma_c$  is the compressive stress,  $\varepsilon_c^{pl}$  is the compressive plastic strain, and the value of  $b_c = 0.7$  was suggested by the authors. The tension degradation property was calculated according to Pavlovi et al. [40] from the following equation:

$$d_t = 1 - \frac{\sigma_t}{\sigma_{t0}} \quad (13)$$

The maximum damage parameters value was taken as 0.9, which accounts for convergence problems related to excessive damage suggested in the ABAQUS user manual [31].

**Reinforcement Model:** The classical metal plasticity model was used for reinforcements. The Mises yield surface was defined, which provides an isotropic hardening behavior. A trilinear elastoplastic stress-strain curve [23] was used, which is based on experimental tensile load test data. Ductile damage

parameters were used in the model to consider the rupture of reinforcement steel. The reinforcement model parameters are given in Table 2.

**Table 2: Material model parameters for reinforcement steel**

Density (kg/m <sup>3</sup> )	Young's modulus (MPa)	Poisson's ratio	Plastic parameters	
7800	200000	0.3	Yield stress	Plastic strain
<b>Ductile damage parameters</b>			508	0
Fracture strain	Stress triaxiality	Strain rate	580	0.0275
0.1	1	1	580	0.0675

**Modelling of Fe-SMA:** The stress-strain curve shown in Figure 1 from the tension test results of Abouali et al. [24] was used to define Fe-SMA's material behaviour with isotropic hardening plasticity. As proposed by Abouali et al. [24], the implementation of the activated behaviour of Fe-SMA strips in ABAQUS was done by considering the loading to failure portion of the curve as input. In this way, when the structure is loaded, the Fe-SMA strips follow the recovery stress and recovery strain path till failure. The recovery stress is induced into the Fe-SMA strips by direct application of prestressing via predefined field stress option in ABAQUS in the axial direction.

**Geometry of Specimen:** Concrete cylinders having 300 mm length and 150 mm diameter is considered for uniaxial compression test, which is the most commonly adopted dimension in India. The standard cylinder has a height/diameter ( $h/d$ ) ratio equal to 2.0. The configuration of the RC bridge pier used in the study is shown in Figure 2. This specimen was replicated as three-dimensional FE model in ABAQUS.

**Boundary Conditions:** The interaction of the assembled bodies and the imposed boundary conditions define the way in which the finite element model will impact both the results and stability of the analysis. For the cylinder specimens, the interactions between the concrete and Fe-SMA strips were modelled as tie constraints. The lower face of the cylinder was restricted from movement in all six degrees of freedom and the upper face was loaded in the axial direction with displacement-controlled loading. The bridge pier

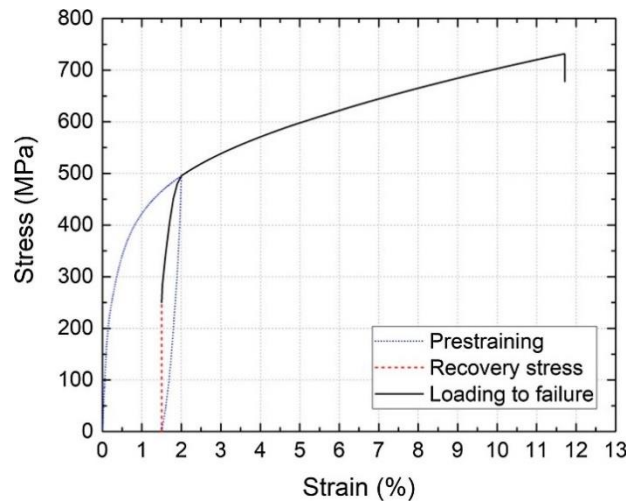


**Fig. 1 Stress-strain curve for activated Fe-SMA [24]**

model essentially consists of three types of interactions. The first is the constraints to prevent rigid body motion, which were externally imposed on the model below the foundation block. It defines the motion of the applicable nodes as zero in all six degrees of freedom. The other one was to load the structure during the course of analysis. The model's loading was done through the vertical surface in the lateral direction of the pier loading head. The pier loading head was constrained as a rigid body. Finally, in order to ensure strain compatibility between the various elements of the FE model, two types of interactions were used. First is the embedded constraint between pier and reinforcement, and second is the tie constraints between pier and Fe-SMA strips, pier and foundation block, and pier and pier loading block.

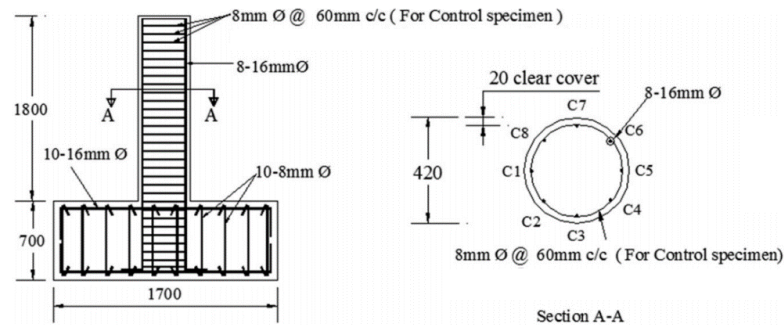


Fig. 2 Reinforcement detailing of the specimen [41]

**Prestressing:** As mentioned earlier, Fe-SMA strips were activated by applying a predefined field initial stress equal to the recovery stress. As per the ABAQUS manual [31], an initial step must be defined without any loading for self-equilibrium of the model. The upward camber as observed in the beam validated the method to application of prestress.

**Loading:** Loading for the uniaxial compression test was applied in two steps. In the first step, the Fe-SMA strips were activated by using predefined field-stress, during which both the top and bottom surfaces of cylinder are free to move vertically and laterally. In the second step, an axial load was applied on the top surface, and the bottom surface was restricted to move in all 6 degrees of freedom. The loading in the pier was applied in three key ways. Initially, the Fe-SMA was activated with no load equilibrium step. The second step was with a fixed axial load of 2.44 kN/m<sup>2</sup> on the top surface of the pier loading head. In the last step, displacement-controlled loading was applied on the two opposite vertical faces of the pier loading head. Implicit analysis in ABAQUS was applied to obtain the non-linear solution.

### 1. Finite Element Model Validation

The Fe-SMA material model behavior, along with the concrete material model, was validated with the experimental results of Shahverdi et al. [23] on near-surface mounted (NSM) strengthening of a reinforced concrete beam with iron-based SMAs. The description of the Fe-SMA NSM beam is shown in Figures 3a and 3c.

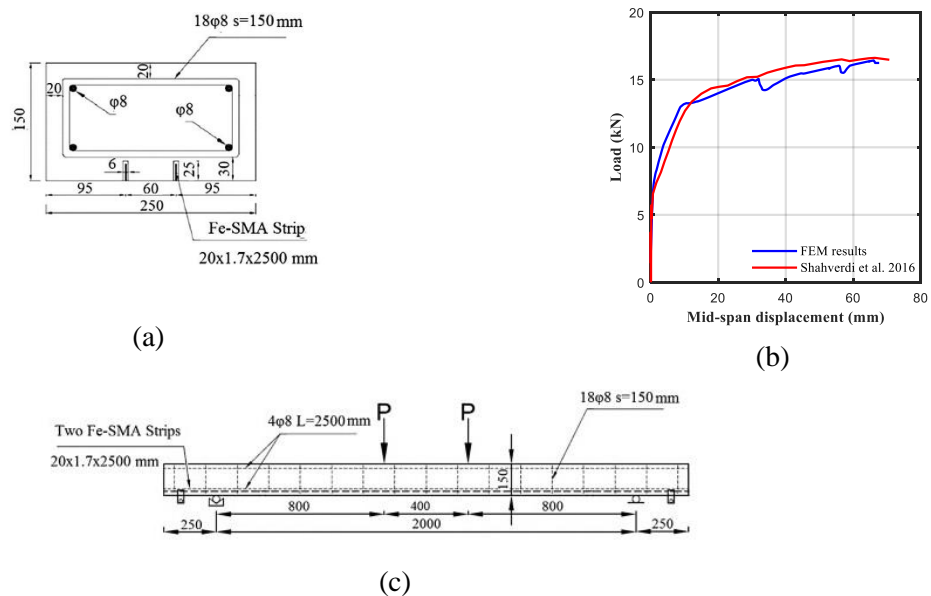


Fig. 3 (a) and (c) Description of experimental NSM strengthened reinforced concrete beam with iron-based SMAs [23], (b) Verification of analytical mode result with experiment result of [23]

Grout was also modelled for near-surface mounting. The CDPM was used for the material model of grout with properties of SikaGrout-311 from Sika, Switzerland [23] with elastic modulus, compressive strength, and tensile strength of 37.2 GPa, 90 GPa, and 3.2 GPa, respectively. The strengthening of the concrete beam using NSM Fe-SMA led to an enhancement of stiffness and load-carrying capacity (about 60%), though originally having an inferior percentage of steel reinforcement. The results of the non-linear analysis indicate that the FE model could reasonably predict the behaviour of the experimental model, as shown in Figure 3b. Hence, the verified modelling strategy was utilized to study the behaviour of SMA retrofitted concrete cylinders and concrete bridge piers.

## 2. Performance Evaluation of Fe-SMA Wrapped Concrete Structures

**Fe-SMA-Confined Concrete Cylinders:** Standard concrete cylinders with a diameter of 150 mm and a height of 300 mm were used in this study to illustrate the effect of Fe-SMA confinement on concrete cylinders under uniaxial monotonic and cyclic compression. Table 3 displays the characteristics of all the specimens and their results in the study. In the specimen labels, “UC25” denotes unconfined specimens, “SMA25” denotes SMA-confined specimens, and the number defines the cube compressive strength of concrete. S1, S2, S3, and S4 indicate four different levels of active confining pressures related to the spacing of 92 mm, 69 mm, 55.2 mm, and 46 mm, respectively. The letter “C” denotes cyclic loading wherever applicable. The loading strain rate of 0.5% /min for monotonic loading, while for cyclically loaded specimens, for the first three cycles, 0.1% followed by eight cycles of 0.4% axial strain was adopted to analyse the behaviour of Fe-SMA-confined concrete cylinders. The cross-section of the Fe-SMA strips used in this study was 24 mm height and 1.5 mm width, and a recovery stress of 250 MPa was applied to all the specimens. The results for the cylinder specimen were calculated at mid-depth to remove the effect of platen restraint. The positive impact of Fe-SMA confinement is clearly evident from the results of the analysis. The results are discussed in the following sections.

**Table 3: Results for monotonically loaded cylinder specimens**

Specimen	Active confinement (MPa)	Axial peak strain	Axial peak stress (MPa)	Residual stress (MPa)
UC25	0	0.0022	19.55	0
SMA25-S1	1	0.0039	29.66	15.01
SMA25-S2	1.48	0.0038	33.86	19.97
SMA25-S3	1.96	0.0069	36.55	26.841
SMA25-S4	2.42	0.0048	45.23	32.749
UC30	0	0.0021	23.46	0
SMA30-S1	1	0.0038	34.14	15.29
SMA30-S2	1.48	0.0038	38.31	20.054
SMA30-S3	1.96	0.0065	40.74	26.997
SMA30-S4	2.42	0.0047	49.50	32.883
UC40	0	0.0023	30.94	0
SMA40-S1	1	0.0037	42.87	15.58
SMA40-S2	1.48	0.0038	47.13	22.096
SMA40-S3	1.96	0.0053	49.22	27.213
SMA40-S4	2.42	0.0045	58.04	32.969
SMA30-S1C	1	0.0040	34.02	14.7
SMA30-S2C	1.48	0.0054	37.67	17.1
SMA30-S3C	1.96	0.0057	40.55	22.34
SMA30-S4C	2.42	0.0052	47.82	36.77

**Effect of Concrete Grade:** Different models of the cylinder with a spacing of Fe-SMA strips of 92 mm, 69 mm, 55.2 mm, and 46 mm were analysed to find the effect of different concrete grades. The comparison of Fe-SMA-confined concrete with different grades and with the same spacing is shown in Figures 4a-4d. It can be observed that an increase of 51%, 45.3%, and 38.9% in peak axial stress for SMA25-S1, SMA30-S1, and SMA40-S1 specimens with respect to unconfined specimen UC25, UC30, and UC40, respectively. An identical axial residual stress can be observed from these specimens' results. It can thus be inferred that the residual stress is independent of concrete grade for Fe-SMA-confined concrete and only depends on the amount of active confinement for normal strength concrete. A similar trend is observed for

the other two groups of specimens as well. The observations are in agreement with the experimental results of Chen et al. [42].

**Effect of Spacing of Fe-SMA Strips:** Numerical analyses were conducted on SMA-confined concrete specimens with different hoop spacing with the same recovery stress. Figures 5a-5c compare the axial stress-strain of unconfined and confined concrete specimens with different spacing. The peak stress values for specimen UC25, SMA25-S1, SMA25-S2, SMA25-S3, and SMA25-S4 were 19.55 MPa, 29.66 MPa, 33.86 MPa, 36.55 MPa, and 45.23 MPa, respectively. With the increment in confinement pressure (0 MPa to 2.42 MPa), it can be observed that the peak stresses of SMA25-S1 to SMA25-S4 increased by 51%, 72.9%, 81.6%, and 130%, respectively as compared to unconfined confined specimen UC25, UC30, and UC40. Further, as established in the earlier section, axial residual stress is a function of the concrete's confinement level. Thus, with an increase in the confinement value of Fe-SMA strips, the residual stress increased. Accordingly, it can be interpreted that the ductility of RC structures can be enhanced if concrete is able to maintain high residual stresses even at high deformations, which indeed is possible with the Fe-SMA confinement technique. It can also be observed that the degradation of the stiffness of Fe-SMA-confined concrete specimens are almost identical for all the grades of concrete considered in this study.

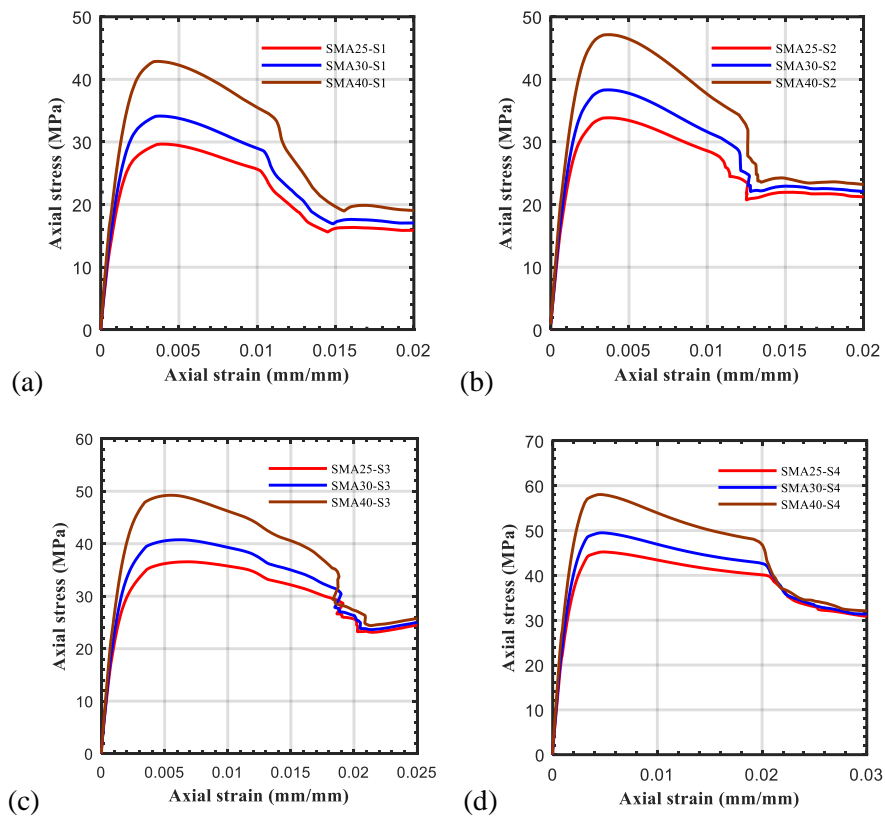


Fig. 4 Effect of concrete grade on Fe-SMA-confined concrete with same active confinement level

**Monotonic vs. Cyclic Loading:** Figure 6 presents axial stress vs. strain of four Fe-SMA-confined cylindrical-shaped concrete specimens. The grade of concrete is 30 MPa, and four different confinement levels of S1, S2, S3, and S4 were considered. The peak stresses were observed to increase by 45.52%, 60.57%, 72.85%, and 103.84%, respectively, compared to that of the unconfined concrete. These test results show that the peak stress and residual stress of concrete specimens confined with SMA increase with the increase in active confining pressure under cyclic loading as well. It could also be observed that the stress-strain curve under monotonic loading closely followed the stress-strain curve under cyclic loading. Essential features like peak stress, slope after the peak, and residual stress were observed to be matching very well with those under monotonic loading. The differences in peak and residual stresses between the stress-strain curve under monotonic and cyclic loading are relatively low and may lead to the conclusion that the former can be considered as an envelope to the later.

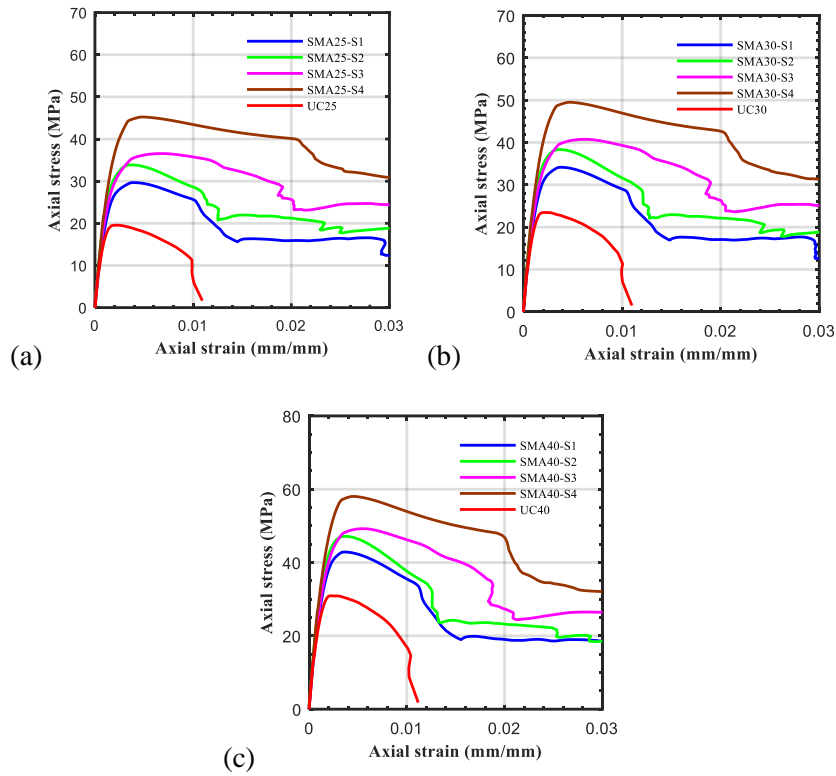


Fig. 5 Effect of different levels of active confinement on axial stress and axial strain relationships of Fe-SMA-confined concrete with the same compressive strength

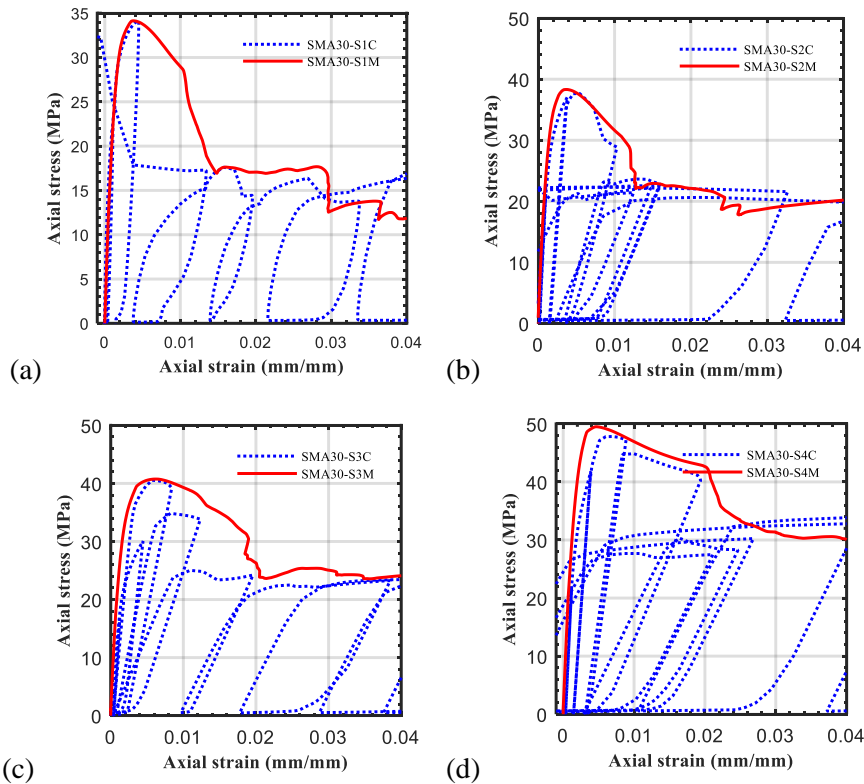


Fig. 6 Axial stress-strain relation for cyclically loaded specimen

**Effect of Height/Diameter ( $h/d$ ) Ratio:** The height of all the cylindrical specimens were kept 300 mm, while the diameters were increased starting from 150 mm up to 600 mm. Two active confinement pressures

of 1 MPa and 2.42 MPa were considered for all the analysed cases. The results are shown in Figure 7. As can be observed from Figures 7b and 7d, when the confining stress is large, the strength of specimens with active confinement is not affected by the size of specimens. As the confining stress is decreased, as shown in Figures 7a and 7c, the strength tends to decrease with increasing specimen size. It can be observed that for actively confined concrete, the strength reduction for 1 MPa active confinement was 14% and for 2.42 MPa was 2.5% as the  $h/d$  ratio is increased to 4. The axial stress-strain curve for all the specimens maintained almost the same pattern throughout the loading process.

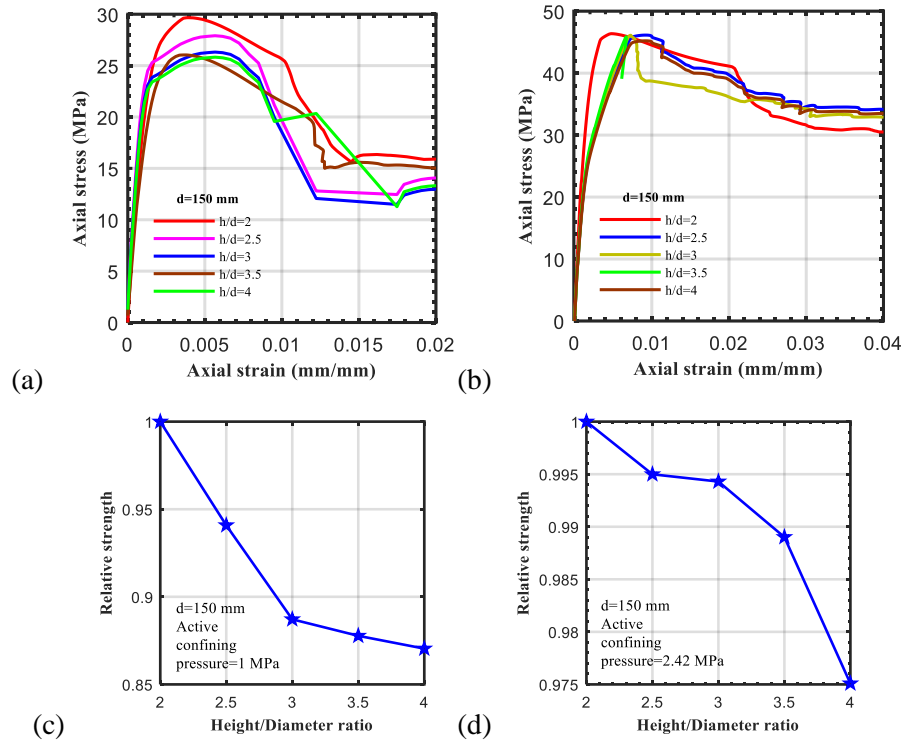


Fig. 7 Influence of height/diameter ratio on Fe-SMA actively confined concrete cylinder strength

**Effect of Size of the Diameter of Specimen:** The cylinder specimens were also analyzed for  $h/d$  ratio = 2 to check the influence of diameter of the specimen with active confining pressure of 1 MPa and 2.42 MPa. The results of axial stress-strain are shown in Figure 8. A similar observation was noticed for the concrete strength of the specimens; with an increase in active confining pressure (Figures 8b and 8d), the strength reduction decreases. Reduction in residual stress was observed with an increase in diameter of the cylinder for both levels of active confinement.

**Dilation Ratio Variation:** Fe-SMA-confined concrete behaves like a combination of active and passive confinement. With the increase in active confining pressure, the contribution from active confinement becomes more prominent. Therefore, the relation between axial-lateral strain relations will provide an idea of actively confined concrete dilation characteristics. The Poisson's ratio describes the typical relation between axial strain and lateral strain which is in the range of 0.15 to 0.22 until the concrete reaches about 70% of its strength [43]. As the loading continued, the concrete continued to dilate for which the dilation ratio increases rapidly and may reach values greater than 0.5 [43]. It is important to investigate the dilation ratio which is defined as the ratio of lateral strain to axial strain. The dilation ratio with respect to axial strain was analyzed for concrete compressive strength of 30 MPa for unconfined concrete and Fe-SMA-confined concrete with different levels of active confinement (S1, S2, S3, and S4). Figure 9 illustrates the evolution of the dilation ratio and axial strain relationship for the different levels of confinement. As the loading starts, all four cases of confinements are observed to start from a dilation ratio of 0.2, and subsequently observed to follow a similar path until a dilation ratio of 0.5 was reached. As can be observed, the unconfined concrete expands more quickly as compared to SP1, SP2, SP3, and SP4. Therefore it can be concluded that the confinement provided by SMA hoops can efficiently support in

deferring the concrete dilation considerably, which therefore attributes to an increase in ductility of concrete. On closer inspection, it can be observed that the dilation ratio is decreasing as the spacing is decreasing from SP1 to SP4. The dilation ratios from all cases were observed to reach stable maximum values at about 1.5 dilation ratio.

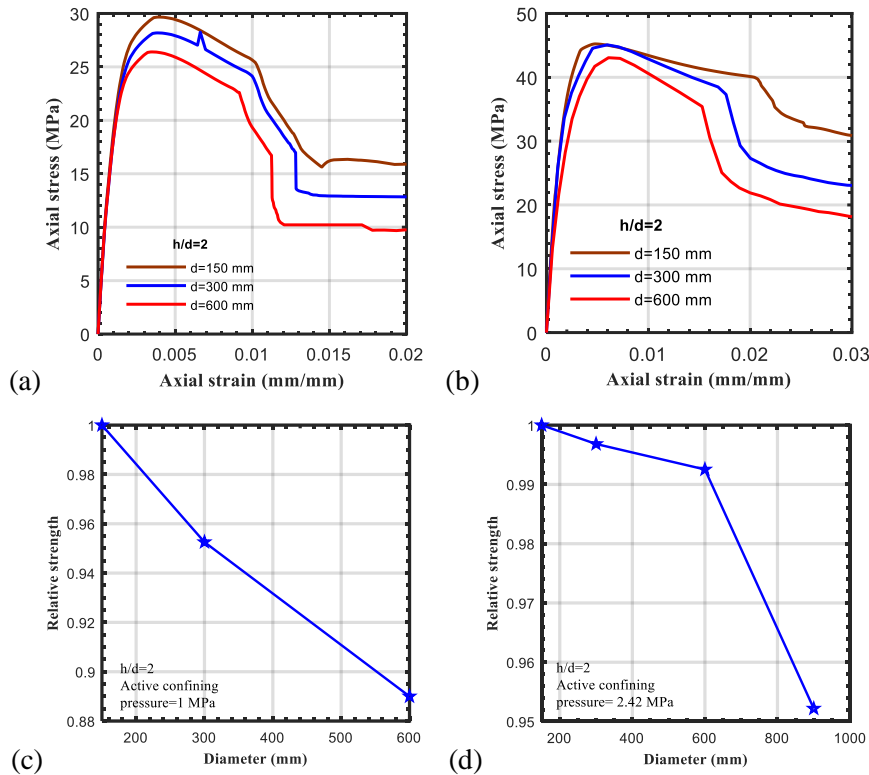


Fig. 8 Influence of diameter on Fe-SMA actively confined concrete cylinder strength

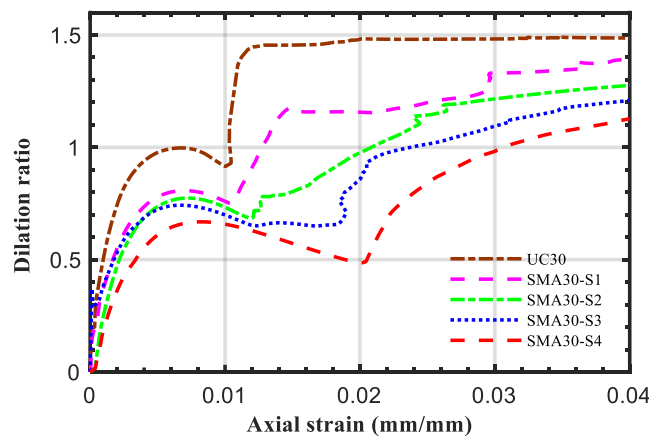


Fig. 9 Effect of increase in active confinement on dilation ratio and axial strain relationship

**Cyclic Loading on Bridge Pier Retrofitted with Fe-SMA:** In this study, a displacement controlled cyclic loading with of 0.5% drift increment was applied to the bridge pier. The study here intends to contribute to the knowledge in the use of Fe-SMA for strengthening RC columns with three different techniques. The first, designated by Near-Surface Mounted (NSM) technique, consists of the insertion of Fe-SMA strips into slits opened on the concrete cover. The second, designated as Externally Bonded (EB) technique, consists of applying of Fe-SMA strips glued and anchored to concrete surface. The third one is external lateral confinement or hoop confinement (HC). To assess the potentialities of the efficiency of these three

techniques in the seismic strengthening, three RC column for each strengthening technique with varying layout schemes were analyzed under cyclic loading. Table 4 shows the parameters used in the strengthening technique.

As can be observed from Figure 10 in terms of initial stiffness, all the strengthened specimens presented similar behaviour, being its degradation much lower than the one revealed by the reference specimen. Table 5 resumes the main results obtained in the performed analysis, while all the curves of Figure 10 depict the response in terms of lateral force versus lateral displacement of the column. All the strengthened specimens presented an increment in the load-carrying capacity when compared to the reference one.

**Table 4: Parameters considered for the strengthening of bridge pier**

Label	Concrete strength (MPa)	
As-built	30	
External lateral confinement	Spacing (mm)	
SMA-HC24	30	24
SMA-HC40	30	40
SMA-HC50	30	50
Near-surface mounted	No. of strips	
SMA-NSM4	30	4
SMA-NSM6	30	6
SMA-NSM8	30	8
Externally bonded	No. of strips	
SMA-EB4	30	4
SMA-EB6	30	6
SMA-EB8	30	8

**Effect of External Lateral Confinement:** The effect of load-displacement relation of external lateral confinement by Fe-SMA strips on bridge piers is shown in Figures 10a, 10b, and 10c. The enhancement of strength for columns retrofitted with hoop confinement for the spacing of 24 mm (SMA-HC24), 40 mm (SMA-HC40), 50mm (SMA-HC50) corresponding to 1.875 MPa, 1.125 MPa, and 0.9 MPa lateral confining pressures have been observed as 28.6%, 24.8%, and 13.8%, respectively. An increase in load-carrying capacity was noticed as the active confinement pressure increased due to decreased spacing of Fe-SMA strips.

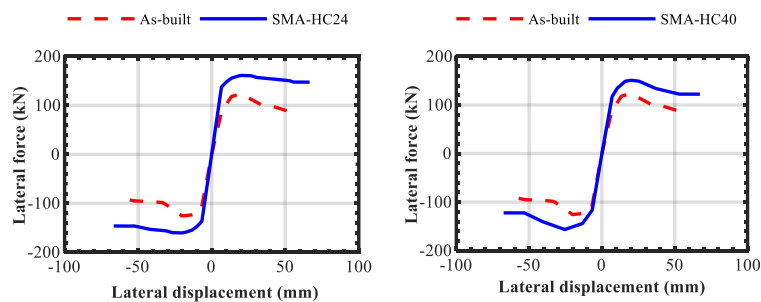
**Effect of Near-Surface Mounted Confinement:** As expected, the specimens strengthened with the NSM technique presented the highest level of performance. Increments of 16.39%, 33.21%, and 38.92% were achieved from SMA-NSM4, SMA-NSM6, and SMA-NSM8, respectively. In the SMA-NSM8, the maximum load was attained, 174.74 kN, which proves the high performance of this technique. The lateral load and lateral displacement relationships, as shown in Figures 10d, 10e, and 10f, indicate that the NSM Fe-SMA retrofitting effectively improved the load-carrying capacity of the bridge piers.

**Effect of Externally Bonded Confinement:** The externally bonded specimens showed an increase in load-carrying capacity. Further, a similar load-displacement pattern was observed as compared to the reference specimen. Figures 10g, 10h, and 10i show the load-displacement curves of externally bonded (EB) specimens with four, six, and eight number of equally spaced Fe-SMA strips mounted on the surface of the column. It can be noticed that as the extent of pre-stressing using EB confinements was increased, the effect on the gain in the load-carrying capacity can also be observed. Figure 10g shows that with lower number of externally bonded strips, no significant increase in capacity could be observed. Therefore, a minimum of 6 externally bonded strips would prove to be an appropriate option. The enhancement of strength for columns retrofitted with EB4, EB6, and EB8 has been observed as 7.5%, 16.6%, and 25.8%, respectively. However, the use of EB SMA strips was observed to be relatively less effective compared to NSM SMA strips. This is due to the fact that NSM arrangements are likely to contribute more as the moment of inertia of SMA strips are higher as compared to EB arrangements with respect to the bending axis.

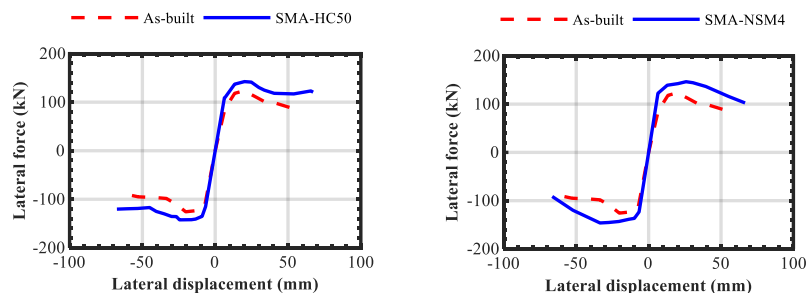
**Table 5: Results for unstrengthened and strengthened bridge pier**

Column	Peak load (kN)	Dissipated energy (kN-m)
AS-built	125.79	2.86
SMA-HC24	161.19	4.66
SMA-HC40	156.51	4.10
SMA-HC50	142.38	3.13
SMA-NSM4	146.41	3.26
SMA-NSM6	167.57	3.39
SMA-NSM8	174.74	3.79
SMA-EB4	135.07	4.52
SMA-EB6	146.05	5.07
SMA-EB8	157.36	5.56
SMA-EB4 & SMA-HC50	169.81	5.67
SMA-NSM4 & SMA-HC50	186.79	5.79

**Combination of Different Fe-SMA Strips' Arrangements:** Two columns were analyzed for a combination of strengthening techniques with Fe-SMA strips. One column with 4-strips mounted with NSM technique (NSM4) and wrapped with 50 mm spacing of external lateral confinement (HC50), and another with 4-strips mounted with EB technique (EB4) and wrapped with external lateral confinement (HC50) of 50 mm spacing. The results for load-displacement are shown in Figures 10j and 10k. At the point of maximum lateral drift (5% drift), a closer comparison reveals an increase in the peak strength of both the combinations relative to other specimens. As expected, the columns with the combination of SMA-NSM4 and SMA-HC50 behaved superior to the combination of EB and HC by a 10% more increment in load-carrying capacity. For SMA-NSM4 and SMA-HC50 combination, the initial stiffness was higher than all other specimens.

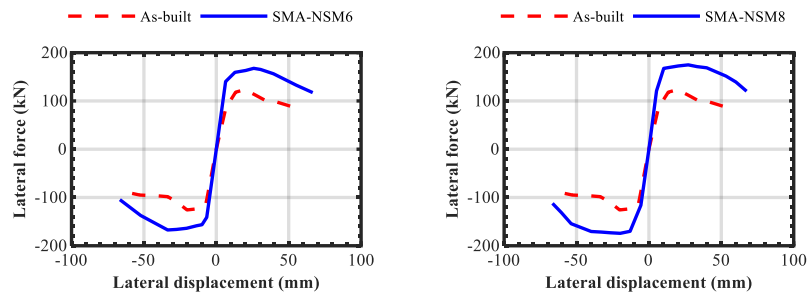


(a) Hoop confinement (24 mm spacing) (b) Hoop confinement (40 mm spacing)



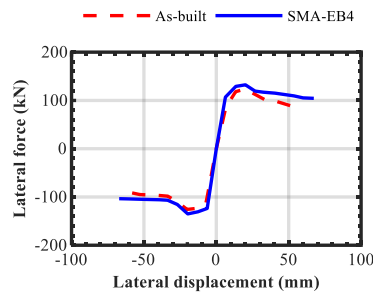
(c) Hoop confinement (50 mm spacing) (d) Near-surface mounted (4 strips)

Fig. 10 Lateral force and lateral displacement relations of as-built and Fe-SMA-confined bridge piers

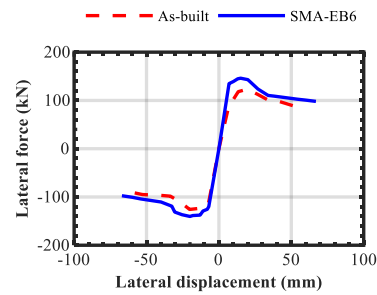


(e) Near-surface mounted (6 strips)

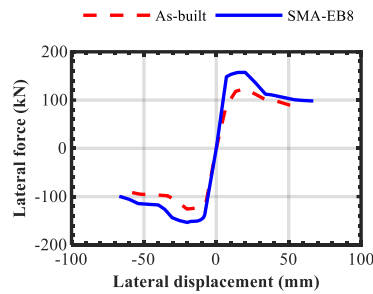
(f) Near-surface mounted (8 strips)



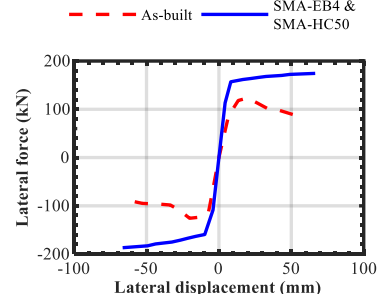
(g) Externally bonded (4 strips)



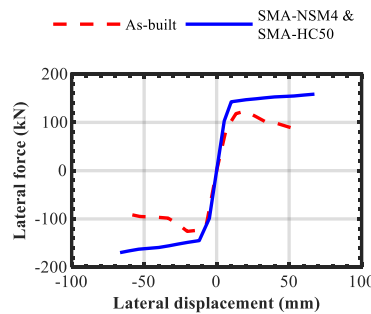
(h) Externally bonded (6 strips)



(i) Externally bonded (8 strips)



(j) Externally bonded (4 strips) with hoop confinement (50 mm spacing)



(k) Near-surface mounted (4 strips) with hoop confinement (50 mm spacing)

Fig. 10 Lateral force and lateral displacement relations of as-built and Fe-SMA-confined bridge piers (continued from previous page)

**CONCLUSION**

The present paper is primarily focused on exploring investigating the applicability of utilizing Fe-SMA as a smart material for retrofit of bridge piers. Finite element based analyses were done using concrete cylinders and RC bridge pier retrofitted with Fe-SMA strips. Different possible configurations using these

strips were attempted, like HC, NSM, and EB and their combinations. The simulated models were analysed under monotonic and cyclic loading. The study conclusively demonstrated superior behaviour of Fe-SMA-confined concrete as compared to normal concrete specimens. The following conclusions are drawn from the present study:

- With the increase in active confining pressure, the efficacy of SMA confinement on concrete in enhancing strength and ductility improves.
- The residual stress of SMA-confined concrete does not depend on the grade of concrete and is predominantly dependent on the level of active confinement.
- The pattern of degradation of stiffness of SMA-confined concrete specimens is same under the same active confining pressure and does not depend on the grade of concrete.
- All the strengthening strategies, namely HC, NSM and EB and their combinations were observed to improve the load-carrying capacity of the considered bridge pier specimen. Increase in energy dissipation was found with increment in level of confinement.
- The best performance in terms of load-carrying capacity was exhibited by SMA-NSM strengthening scheme among all the three variants for the considered bridge pier specimen.

## REFERENCES

1. Paulay, T. and Priestley, M.N. (1992). "Seismic Design of Reinforced Concrete and Masonry Buildings".
2. Richart, F.E., Brandtæg, A. and Brown, R.L. (1928). "A Study of the Failure of Concrete Under Combined Compressive Stresses", *University of Illinois at Urbana Champaign, College of Engineering, Engineering Experiment Station*.
3. Sheikh, S.A. and Uzumeri, S.M. (1982). "Analytical Model for Concrete Confinement in Tied Columns", *Journal of the Structural Division, Vol. 108, No. 12, pp. 2703-2722*.
4. Mander, J.B., Priestley, M.J. and Park, R. (1988). "Theoretical Stress-Strain Model for Confined Concrete", *Journal of Structural Engineering, Vol. 114, No. 8, pp. 1804-1826*.
5. Yu, T.T.J.G., Teng, J.G., Wong, Y.L. and Dong, S.L. (2010). "Finite Element Modeling of Confined Concrete-I: Drucker-Prager Type Plasticity Model", *Engineering Structures, Vol. 32, No. 3, pp. 665-679*.
6. Belal, M.F., Mohamed, H.M. and Morad, S.A. (2015). "Behavior of Reinforced Concrete Columns Strengthened by Steel Jacket", *HBRC Journal, Vol. 11, No. 2, pp. 201-212*.
7. Madas, P. and Elnashai, A.S. (1992). "A New Passive Confinement Model for the Analysis of Concrete Structures Subjected to Cyclic and Transient Dynamic Loading", *Earthquake Engineering & Structural Dynamics, Vol. 21, No. 5, pp. 409-431*.
8. Kotsovos, M.D. and Perry, S.H. (1986). "Behaviour of Concrete Subjected to Passive Confinement", *Materials and Structures, Vol. 19, No. 4, pp. 259-264*.
9. Rousakis, T.C. and Tourtouras, I.S. (2014). "RC Columns of Square Section-Passive and Active Confinement with Composite Ropes", *Composites Part B: Engineering, Vol. 58, pp. 573-581*.
10. Rousakis, T.C. and Tourtouras, I.S. (2015). "Modeling of Passive and Active External Confinement of RC Columns with Elastic Material", *ZAMM-Journal of Applied Mathematics and Mechanics/ Zeitschrift für Angewandte Mathematik und Mechanik, Vol. 95, No. 10, pp. 1046-1057*.
11. Holmes, N., Niall, D. and O'shea, C. (2015). "Active Confinement of Weakened Concrete Columns", *Materials and Structures, Vol. 48, No. 9, pp. 2759-2777*.
12. Saatcioglu, M. and Yalcin, C. (2003). "External Prestressing Concrete Columns for Improved Seismic Shear Resistance", *Journal of Structural Engineering, Vol. 129, No. 8, pp. 1057-1070*.
13. Nesheli, K.N. and Meguro, K. (2006). "Seismic Retrofitting of Earthquake-Damaged Concrete Columns by Lateral Pre-Tensioning of FRP Belts", *In Proceedings of the Eighth US National Conference on Earthquake Engineering*.
14. Lagoudas, D.C. (Ed.). (2008). "Shape Memory Alloys: Modeling and Engineering Applications", *Springer Science & Business Media*.

15. Dong, Z., Klotz, U.E., Leinenbach, C., Bergamini, A., Czaderski, C. and Motavalli, M. (2009). "A Novel Fe-Mn-Si Shape Memory Alloy with Improved Shape Recovery Properties by VC Precipitation", *Advanced Engineering Materials*, Vol. 11, No. 1-2, pp. 40-44.
16. Andrawes, B. and Shin, M. (2008). "Seismic Retrofit of Bridge Columns Using Innovative Wrapping Technique", *In Structures Congress 2008: Crossing Borders*, pp. 1-10.
17. Andrawes, B. and Shin, M. (2010). "Experimental Investigation of Concrete Columns Wrapped with Shape Memory Alloy Spirals", *In Improving the Seismic Performance of Existing Buildings and other Structures*, pp. 835-840.
18. Shin, M. and Andrawes, B. (2011). "Emergency Repair of Severely Damaged Reinforced Concrete Columns Using Active Confinement with Shape Memory Alloys", *Smart Materials and Structures* Vol. 20, No. 6, pp. 065018.
19. Shin, M. and Andrawes, B. (2010). "Experimental Investigation of Actively Confined Concrete Using Shape Memory Alloys", *Engineering Structures*, Vol. 32, No. 3, pp. 656-664.
20. Chen, Q. and Andrawes, B. (2014). "Finite Element Analysis of Actively Confined Concrete Using Shape Memory Alloys", *Journal of Advanced Concrete Technology*, Vol. 12, No. 12, pp. 520-534.
21. Shahverdi, M., Michels, J., Czaderski, C. and Motavalli, M. (2018). "Iron-Based Shape Memory Alloy Strips for Strengthening RC Members: Material Behavior and Characterization", *Construction and Building Materials*, Vol. 173, pp. 586-599.
22. Lee, W.J., Weber, B., Feltrin, G., Czaderski, C., Motavalli, M. and Leinenbach, C. (2013). "Phase transformation Behavior Under Uniaxial Deformation of an Fe-Mn-Si-Cr-Ni-VC Shape Memory Alloy", *Materials Science and Engineering: A*, Vol. 581, pp. 1-7.
23. Shahverdi, M., Czaderski, C. and Motavalli, M. (2016). "Iron-Based Shape Memory Alloys for prestressed Near-Surface Mounted Strengthening of Reinforced Concrete Beams", *Construction and Building Materials*, Vol. 112, pp. 28-38.
24. Abouali, S., Shahverdi, M., Ghassemieh, M. and Motavalli, M. (2019). "Nonlinear Simulation of Reinforced Concrete Beams Retrofitted by Near-Surface Mounted Iron-Based Shape Memory Alloys", *Engineering Structures*, Vol. 187, pp. 133-148.
25. Fritsch, E., Izadi, M. and Ghafoori, E. (2019). "Development of Nail-Anchor Strengthening System with iron-Based Shape Memory Alloy (Fe-SMA) Strips", *Construction and Building Materials*, Vol. 229, pp. 117042.
26. Ghafoori, E., Neuenschwander, M., Shahverdi, M., Czaderski, C. and Fontana, M. (2019). "Elevated Temperature Behavior of an Iron-Based Shape Memory Alloy Used for Prestressed Strengthening of Civil Structures", *Construction and Building Materials*, Vol. 211, pp. 437-452.
27. Li, L., Chen, T., Gu, X. and Ghafoori, E. (2020). "Heat Activated SMA-CFRP Composites for Fatigue Strengthening of Cracked Steel Plates", *Journal of Composites for Construction*, Vol. 24, No. 6, pp. 04020060.
28. Raad, J. and Parvin, A. (2020). "Iron-Based Shape Memory Alloy and Fiber Reinforced Polymers Rods for Prestressed NSM Strengthening of RC Beams", *Engineering Structures*, Vol. 207, pp. 110274.
29. Cladera, A., Montoya-Coronado, L.A., Ruiz-Pinilla, J.G. and Ribas, C. (2020). "Shear Strengthening of Slender Reinforced Concrete T-Shaped Beams Using Iron-Based Shape Memory Alloy Strips", *Engineering Structures*, Vol. 221, pp. 111018.
30. Gebreyohannes, A.S., Clifton, G.C. and Butterworth, J.W. (2012). "Finite Element Modeling of Non-Ductile RC Walls", *In Proceedings of the Fifteenth World Conference on Earthquake Engineering*.
31. Hibbitt, K. (2013). "ABAQUS: User's Manual: Version 6.13", pp. 369-372.
32. Lundqvist, J., Nordin, H., Täljsten, B. and Olofsson, T. (2005). "Numerical Analysis of Concrete Beams Strengthened with CFRP: a Study of Anchorage Lengths", *In International Symposium on Bond Behaviour of FRP in Structures*, International Institute for FRP in Construction, pp. 239-246.
33. Lubliner, J., Oliver, J., Oller, S. and Oñate, E. (1989). "A Plastic-Damage Model for Concrete", *International Journal of Solids and Structures*, Vol. 25, No. 3, pp. 299-326.
34. Lee, J. and Fenves, G.L. (1998). "Plastic-Damage Model for Cyclic Loading of Concrete Structures", *Journal of Engineering Mechanics*, Vol. 124, No. 8, pp. 892-900.

35. CEB-FIP Model Code (1990). "London: Thomas Telford Ltd: Comité Euro-International de Béton; n.d".
36. Hognestad, E. (1951). "Study of Combined Bending and Axial Load in Reinforced Concrete Members", *University of Illinois at Urbana Champaign, College of Engineering. Engineering Experiment Station.*
37. Stoner, J. (2015). "Finite Element Modelling of GFRP Reinforced Concrete Beams", *MS Thesis, University of Waterloo.*
38. Cornelissen, H., Hordijk, D. and Reinhardt, H. (1986). "Experimental Determination of Crack Softening Characteristics of Normal Weight and Light Weight", *Heron, Vol. 31, No. 2, pp. 45-46.*
39. Birtel, V. and Mark, P. (2006). "Parameterised Finite Element Modelling of RC Beam Shear Failure", *ABAQUS Users' Conference, Vol. 14.*
40. Pavlovic, M., Markovic, Z., Veljkovic, M. and Budevac, D. (2013). "Bolted Shear Connectors vs. Headed Studs Behaviour in Push-Out Tests", *Journal of Constructional Steel Research, Vol. 88, pp. 134-149.*
41. Kotoky, N., Dutta, A. and Deb, S.K. (2019). "Comparative Study on Seismic Vulnerability of Highway Bridge with Conventional and HyFRC Piers", *Bulletin of Earthquake Engineering, Vol. 17, No. 4, pp. 2281-2306.*
42. Qiwen, C. and Andrawes, B. (2017). "Cyclic Stress–Strain Behavior of Concrete Confined with NiTiNb-Shape Memory Alloy Spirals", *Journal of Structural Engineering, Vol. 143, No. 5, pp. 04017008.*
43. Mirmiran, A. and Shahawy, M. (1997). "Dilation Characteristics of Confined Concrete", *Mechanics of Cohesive-frictional Materials: An International Journal on Experiments, Modelling and Computation of Materials and Structures, Vol. 2, No. 3, pp. 237-249.*